Journal of The Electrochemical Society, 2022 **169** 044523

Accelerated Durability Testing of Fuel Cell Stacks for Commercial Automotive Applications: A Case Study

Tsuyoshi Takahashi,[1,2] Takuya Ikeda,[1] Kazuya Murata,[1] Osamu Hotaka,[1] Shigeki Hasegawa,[1] Yuya Tachikawa,[3,4] Masamichi Nishihara,[4] Junko Matsuda,[3,4] Tatsumi Kitahara,[2] Stephen M. Lyth,[3,5,6] Akari Hayashi,[2,3,4,5,*] and Kazunari Sasaki[2,3,4,5,*,z]

[1]*Commercial ZEV System Products Development Division, Toyota Motor Corporation, Toyota Aichi, 471-8571, Japan*
[2]*Department of Hydrogen Energy Systems, Faculty of Engineering, Kyushu University, Nishi-ku Fukuoka 819-0395, Japan*
[3]*International Research Center for Hydrogen Energy, Kyushu University, Nishi-ku Fukuoka 819-0395, Japan*
[4]*Next-Generation Fuel Cell Research Center (NEXT-FC), Kyushu University, Nishi-ku Fukuoka 819-0395, Japan*
[5]*Platform of Inter-/Transdisciplinary Energy Research (Q-PIT), Kyushu University, Nishi-ku Fukuoka 819-0395, Japan*
[6]*Department of Automotive Science, Graduate School of Integrated Frontier Sciences, Kyushu University, Nishi-ku Fukuoka 819-0395, Japan*

System durability is crucially important for the successful commercialization of fuel cell electric vehicles (FCEVs). Conventional accelerated durability testing protocols employ relatively high voltage to hasten carbon corrosion and/or platinum catalyst degradation. However, high voltages are strictly avoided in commercialized FCEVs such as the Toyota MIRAI to minimize these degradation modes. As such, conventional durability tests are not representative of real-world FCEV driving conditions. Here, modified start-stop and load cycle durability tests are conducted on prototype fuel cell stacks intended for incorporation into commercial FCEVs. Polarization curves are evaluated at beginning of test (BOT) and end of test (EOT), and the degradation mechanisms are elucidated by separating the overvoltages at both 0.2 and 2.2 A cm^{-2}. Using our modified durability protocols with a maximum cell voltage of 0.9 V, the prototype fuel cell stacks easily meet durability targets for automotive applications, corresponding to 15-year operation and 200,000 km driving range. These findings have been applied successfully in the development of new fuel cell systems for FCEVs, in particular the second-generation Toyota MIRAI.
 [DOI: 10.1149/1945-7111/ac662d]

Manuscript submitted December 13, 2021; revised manuscript received April 6, 2022. Published April 20, 2022.

It is increasingly evident that technical innovation is required to preserve the natural environment and achieve a carbon-neutral society. Electrification is being heavily promoted in the automobile industry as part of the "connected, autonomous, shared, electric" (CASE) concept. Hydrogen fuel cells are becoming a core technology in the journey towards automobile electrification,[1–3] and the International Energy Agency (IEA) highlighted their importance in its recent "*Future of Hydrogen*" report.[4] Toyota began commercialization of their MIRAI FCEV in 2014,[5–9] and the 2nd generation MIRAI was released in December 2020. Figure 1 shows photographs of (a) the fuel cell system and (b) a single cell (sectioned to display the different components) employed in the 2nd generation MIRAI.[10–13]

Sufficient reliability and durability are essential for the popularization of FCEVs as competitive commercial products.[14,15] Many reports in the literature have focused on durability issues such as gas crossover through the electrolyte membrane; gas leakage from fuel cell stacks; and general deterioration of cell performance.[16–18] Clarification and resolution of issues pertaining to the durability are important for the development of next generation FCEVs.

Major factors in the deterioration of fuel cell performance are related to the electrocatalyst layer. Sources of performance degradation include: (i) platinum dissolution due to the fluctuating cell voltage; (ii) nanoparticle aggregation due to weak metal-support interaction; (iii) Ostwald ripening due to repeated Pt dissolution and redeposition on larger and more thermodynamically stable nanoparticles; and (iv) electrode thinning via oxidation and gasification of the carbon support at a high voltage.[14–18]

The typical required lifetime of a commercial passenger vehicles is around 15 years, and the total driving distance is around 200,000 km. It is clearly impractical to test fuel cell stacks for that long, therefore the durability of fuel cell systems is generally investigated using accelerated stress tests. Such tests have been standardized by e.g. the United States Fuel Cell Council (US FCC) and the United States Department of Energy (US DOE).[19] Meanwhile, the Fuel Cell Commercialization Conference of Japan (FCCJ); the New Energy and Industrial Technology Development Organization (NEDO); and the Japan Automobile Research Institute (JARI) have also proposed their own standardized evaluation protocols in Japan.[20,21] These protocols have been extremely useful when applied extensively in the literature to evaluate the performance of e.g. alternative electrode materials; novel membranes; reduction of platinum loading; and/or evaluation of degradation mechanisms.[21–27] These types of study have proved valuable in understanding and improving fuel cell performance, especially the degradation mechanisms. However, in most cases these studies deal with single cells. When considering mass-production and commercialization in products such as FCEVs, fuel cell stacks should also be subjected to accelerated stress tests. There have been various studies investigating the durability of fuel cell stacks,[28–30] but to the best our knowledge, accelerated stress tests of fuel cell stacks intended for commercial FCEV applications have not yet been reported.

The experimental conditions for durability tests of commercial fuel cell stacks should be determined based on realistic driving behaviors, and the actual specifications of FCEV systems. Under real-world driving conditions, there are many interdependent and complicated factors which can cause the deterioration of fuel cell systems. The development of durable fuel cell products requires two different approaches: (i) the development of durable materials which can survive in severe conditions; and (ii) the design of suitable operating systems which avoid severe conditions wherever possible.

In this work, we employ modified durability test protocols considering both approaches. The in-house evaluation protocols reported in this study are therefore different in some respects from those recommended by the organizations mentioned earlier. For example, durability protocols defined by the US DOE and the FCCJ

*Electrochemical Society Member.
[z]E-mail: sasaki@mech.kyushu-u.ac.jp

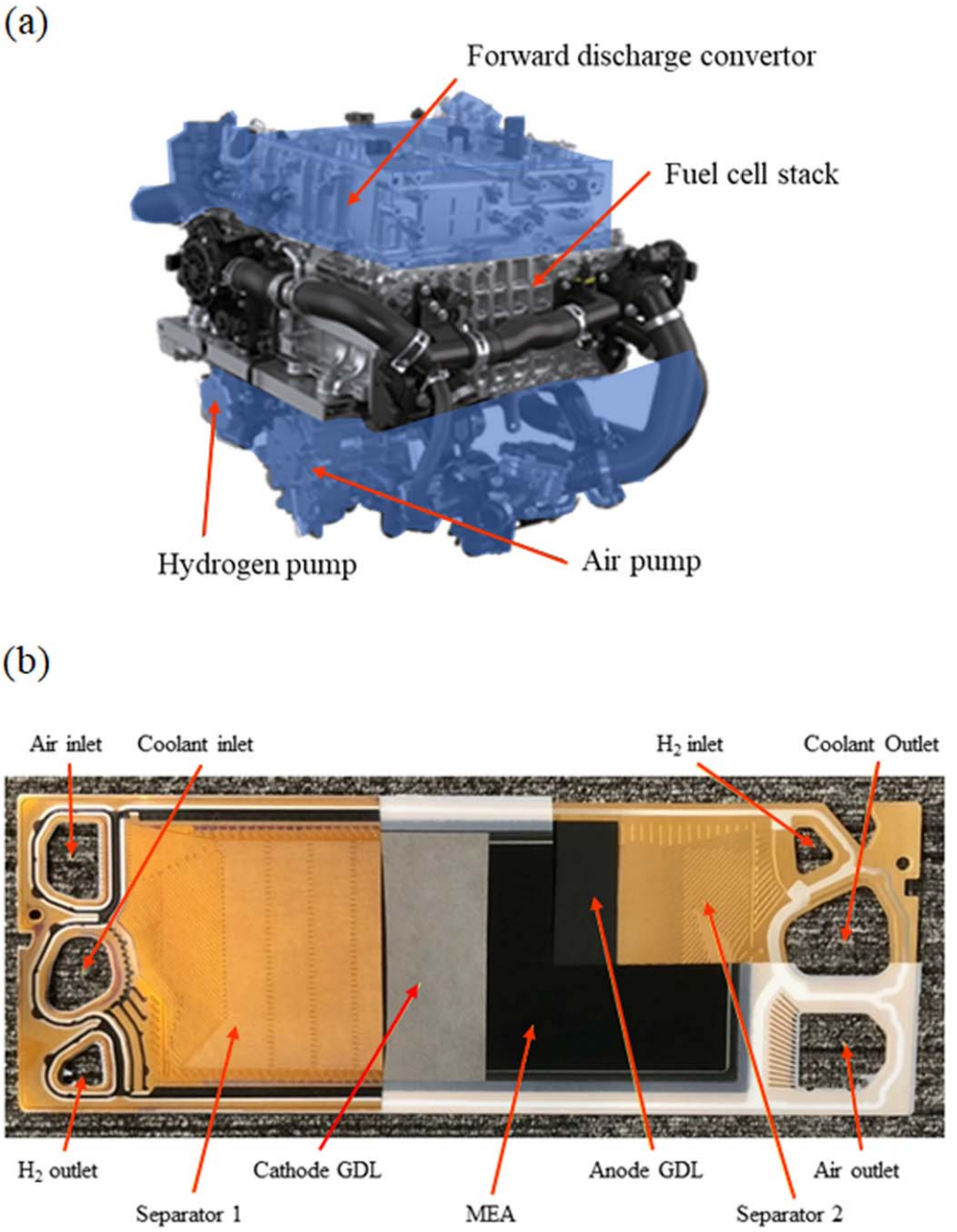

Figure 1. The fuel cell system of the 2nd generation Toyota MIRAI.[10–13] (a) Fuel cell stack assembly and balance of plant. (b) Single fuel cell module including the membrane electrode assembly (MEA) and separators.

recommend the use of nitrogen gas at the cathode to improve the accuracy and reproducibility of the resulting data.[19–21] In contrast, we use air because the effect of water generation at the cathode must also be considered in commercial FCEV systems. Furthermore, the FCCJ protocols recommend repeated potential cycling up to 1.0 V in case of the load cycle durability tests to accelerate platinum catalyst degradation processes, and at cell voltages up to 1.5 V to accelerate carbon support oxidation.[20–24,31–34] However, in commercial FCEV systems such as the Toyota MIRAI, the system is carefully designed such that the cell voltage always remains below 0.9 V specifically to avoid degradation via these mechanisms. The durability protocols presented in this work therefore reflect these considerations.

There is a serious demerit in limiting the cell voltage during FCEV operation, since the efficiency is intimately linked with the cell voltage. However, this issue can be managed effectively by the FCEV operating system. For example, if the voltage of the fuel cell stack drops, leading to lower efficiency, the on-board lithium-ion battery can be employed to temporarily support its operation.

The above concerns about efficiency are also offset by the highly beneficial effect on durability. For example, the drop in power output after accelerated load cycle tests has previously been evaluated in-house for different values of the upper limiting cell voltage, as shown in Fig. 2 (all measurements were made at a current density of 0.8 A cm^{-2}).[35] In this figure, the drop in power output is normalized, with 0 corresponding to the initial power output, and 1.0 corresponding to the largest observed drop in power output after accelerated stress testing at a given upper limiting cell voltage. The output power drop was highest after testing up to 1.0 V, indicating the highest degree of degradation. However, slightly decreasing the upper voltage limit to 0.90 V results in significantly lower normalized output drop of just 0.35. As such, it is evident that restricting the upper voltage limit to $\leqslant$0.9 V will dramatically slow

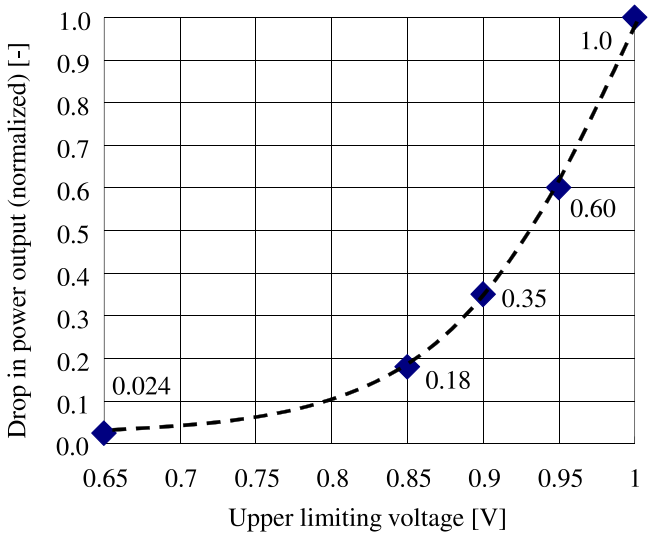

Figure 2. Relationship between the upper limiting voltage and the normalized drop in power output after load cycle durability tests.[35] Power outputs were measured at 0.8 A cm^{-2} in all cases, and the total number of load cycles was 48,240. A value of 0.0 corresponds to the power output at beginning of test (BOT), and a value of 1.0 corresponds to the maximum observed drop in power output at end of the test (EOT).

the rate of performance loss. Based on such considerations, the upper limiting cell voltage is fixed at ⩽0.9 V throughout this study.

Overall, the aim of this study is to investigate the degradation of prototype fuel cell stacks, using modified accelerated stress tests designed to simulate realistic driving conditions in commercial FCEV systems.

Experimental

Prototype fuel cell stack design.—The prototype stack prepared for this study consisted of 13 single cells, and was designed and built in-house by Toyota Motor Corporation. Each cell comprised a membrane electrode assembly (MEA) sandwiched between carbon paper gas diffusion layers (GDLs, Toray, Japan), and bespoke titanium-based separators as shown in Fig. 1b.[10,11,36] The separators have patterned gas channels, and are coated with a titanium oxide (TiO_x) and carbon nanocomposite layer.[10–13] The cell was consolidated using a proprietary three-layer sheet comprising thermoplastic materials, acting as both a gasket to prevent leakage and glue to bond the components together.[11,36] This sheet helps to significantly shorten the stack manufacturing process. Mesoporous carbon nano-dendrites (MCND)[11,37] were used as a catalyst support at the cathode, and these materials were decorated with Pt-Co alloy catalysts.[11,36] Meanwhile Pt catalysts supported on carbon black were used at the anodes. The Pt loading was 0.17 mg-Pt cm^{-2} at the cathode, and 0.025 mg-Pt cm^{-2} at the anode. A proprietary ionomer with three times higher oxygen permeability compared to conventional Nafion ionomers was used in the electrocatalyst layers.[11,38] Figure 3 shows a schematic image of the fuel cell stack. Each cell was numbered sequentially from 1 at the negative terminal to 13 at the positive terminal. For evaluation of temperature and voltage, we used a dummy cell next to the positive terminal to avoid external thermal disturbance. The hydrogen and air gas inlets were both located at the positive terminal side of the stack, and these gases were separately supplied to the anode and cathode via a flow field. Coolant (a mixture of water and ethylene glycol) was introduced through a separate flow field system.

Stack durability test conditions.—Our in-house experience indicates that the peak to average power ratio for a mid-size vehicle in normal city driving conditions is slightly over 10:1. Meanwhile, FCEVs are powered by a hybrid vehicle power-train system which includes a lithium-ion battery, and the maximum and average power outputs depend on the balance between the fuel cell and battery. As such, a peak to average power ratio of 12% was used in this study, as a practical target for commercial FCEV systems. Practically, this means that the voltage drop during accelerated durability tests was evaluated at 2.2 A cm^{-2} corresponding to the maximum power density, as well as at 0.2 A cm^{-2} corresponding to 12% of the maximum power density, or "average" driving conditions.

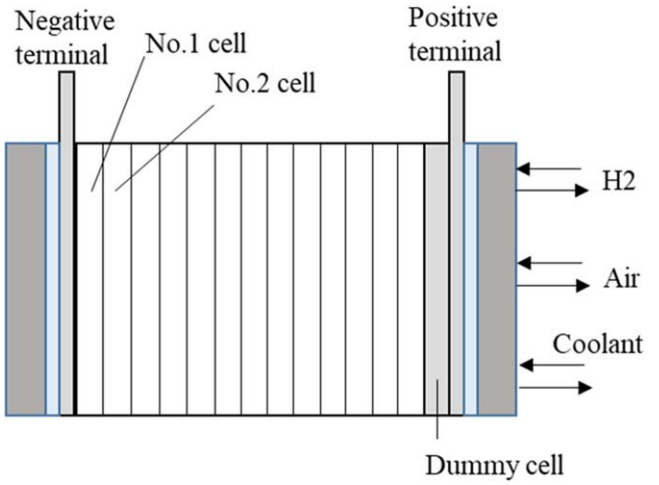

Figure 3. Schematic diagram of the fuel cell stack comprising 13 numbered cells.

Start-stop durability test.—Start-stop operation of passenger vehicles (i.e. switching the engine on and off) is normally performed about five times a day on average according to recent market surveys performed in-house, in agreement with publicly available data.[39] This corresponds to almost 30,000 start-stop cycles over the 15-year lifetime of a consumer vehicle. Based on these considerations, along with typical FCEV operating conditions, the fuel cell stack was subjected to 30,000 voltage cycles between 0.05 V and 0.88 V over the course of the test. Regarding the ramp rate, the time taken between the minimum cell voltage (0.05 V) and the maximum cell voltage (0.88 V) was 2 s, corresponding to 0.415 V s^{-1}, which are the same conditions as used in real FCEV system operation. The cycling protocol for these accelerated start-stop durability tests is shown in Fig. 4a, and the detailed experimental conditions are outlined in Table I. The stack temperature in the start-stop durability tests was controlled by the coolant which was set at 57 °C, although it should be noted that operation at lower temperatures could accelerate voltage degradation by e.g. liquid water formation. In one cycle, the voltage was held at 0.88 V for 30 s then at around 0.05 V for 18 s. These holding times were determined based on previous research.[40]

Load cycle durability test.—The load cycling protocol and experimental conditions are summarized in Fig. 4b and Table II, respectively, based on the typical operating conditions of an FCEV and the results of in-house behavioral market surveys. In one cycle, the cell voltage was held at 0.6 V for 10 s and then held at 0.9 V for 15 s. Regarding ramp rate, the time taken between the maximum power output (0.6 V) and the minimum power output (0.9 V) was 2 s, corresponding to 0.15 V s^{-1}, which are the same conditions used in real FCEV system operation. The fuel cell stack was subjected to a total of 73,000 load cycles. This corresponds to an average of one load cycle per 2 to 3 km of driving (or one acceleration event requiring higher current density/lower cell voltage). The stack temperature in this case was controlled by the coolant to be 70 °C, which is a typical operation temperature.

Real commercial FCEV systems such as the MIRAI do not employ a humidifier, and therefore the accelerated stress testing

Table I. Experimental conditions for the accelerated start-stop durability tests.

		Voltage [V]		Time [s]
Cell voltage and operation time	Lower	0.05		18
	Upper	0.88		30
Cell temperature [°C]			57	
Number of cycles			30,000	
Flow rate [L min^{-1}]	Anode		6.7	
	Cathode		23.2	
Gas temperature [°C]	Anode		80	
	Cathode		80	
Dew point [°C]	Anode		65	
	Cathode		65	
Gas pressure (stack outlet) [kPa absolute]	Anode		200	
	Cathode		100	

Table II. Experimental conditions for the accelerated load cycle durability tests.

		Voltage [V]		Time [s]
Cell voltage and operation time	Lower	0.6		10
	Upper	0.9		15
Cell temperature [°C]			70	
Number of cycles			73,000	
Flow rate (Stoichiometry)	Anode		1.45	
	Cathode		1.45	
Gas temperature [°C]	Anode		80	
	Cathode		80	
Dew point [°C]	Anode		45	
	Cathode		53	
Gas pressure (stack outlet) [kPa absolute]	Anode		240	
	Cathode		140	

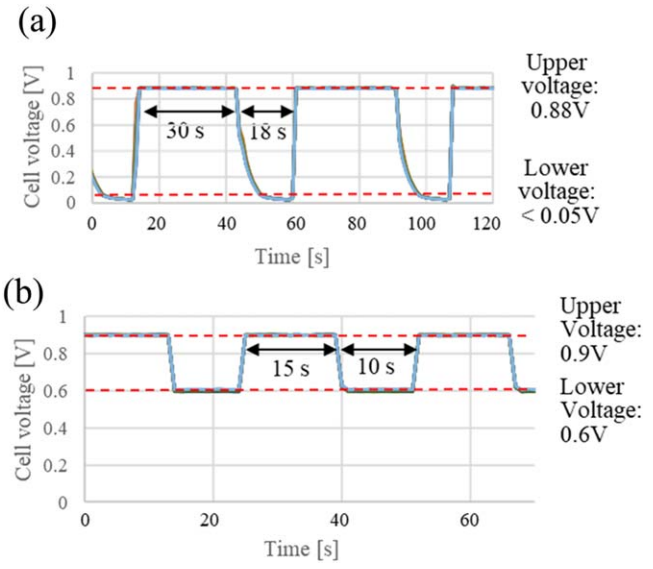

Figure 4. Durability test protocols for (a) start-stop and (b) load cycle operation.

protocols reflect this. As such, the relative humidity in these tests may be significantly lower than used in conventional load cycling protocols, in which the higher relative humidity may result in e.g. accelerated degradation via Pt dissolution. In this study, the load cycle durability test was carried out immediately after the start-stop durability test to help understand the overall durability of the fuel cell system in FCEVs.

IR-free polarization curve measurements.—Polarization curves were measured both at beginning of test (BOT) and end of test (EOT). Experimental conditions are summarized Table III. Impedance was measured by an impedance analyzer (BT3562, HIOKI, Japan). The frequency for impedance measurements was 1 kHz ± 0.2 Hz, and the current range was from 10 μA to 100 mA. IR losses were calculated from the impedance data, and the IR-free voltage was then obtained by adding the IR losses to the measured cell voltage.

SEM observation of the electrocatalyst layer and crystallite size analysis.—The microstructure of the electrocatalyst layers at BOT and EOT were observed by scanning electron microscopy (SEM, S-4800, Hitachi High–Technologies, Japan) with an acceleration voltage of 2.0 kV. Secondary electron images were recorded. Catalyst nanoparticle size was estimated from the crystallite size as determined by X-ray diffraction (XRD, SmartLab, Rigaku, Japan). Crystallite size was calculated from the half width of Pt (220) XRD peak using the Scherrer formula. XRD measurements were performed at an acceleration voltage of 40 kV and a current of 40 mA, in a 2θ range from 20 to 90°, at a scanning rate of 2° per min, with a sampling width of 0.02°.

Cyclic voltammograms of fuel cells.—Cyclic voltammetry (CV) was applied for a representative cell within the 13-cell stacks. Before CV measurements, a 30-min pretreatment was performed to achieve stable cell conditions. In this step, hydrogen gas was supplied to the anode at a flow rate of 2 NL min^{-1}, at 200 kPa absolute pressure, and humidified at 50 °C (i.e., the dew point). Meanwhile, nitrogen gas was supplied to the cathode at a flow rate of 4 NL min^{-1}, at atmospheric pressure (100 kPa absolute), and humidified at 50 °C (i.e., the dew point). The cell temperature was 30 °C. After 30 min, the hydrogen and nitrogen supplies were stopped and CV

Table III. Experimental conditions for polarization curve measurements: the gas temperature (H_2, air) was 80 °C; the gas dew-point was 45 °C for H_2 and 0 °C for air; and the coolant temperature was 55 °C at the inlet, and 70 °C at the outlet.

	Gas flow-rate (Stoichiometry)		Gas inlet pressure [kPa abs]	
Current density [A cm^{-2}]	H_2	Air	H_2	Air
2.2	1.25	1.5	220	220
2.0	1.25	1.5	220	220
1.7	1.25	1.5	220	200
1.5	1.25	1.5	210	180
1.1	1.25	1.5	190	160
1.0	1.25	1.5	190	160
0.7	1.25	1.5	170	130
0.5	1.8	1.5	170	110
0.2	2.2	1.5	160	110
0.1	2.2	2.0	160	110
0.05	2.5	2.6	150	110

measurements were conducted in the closed environment at 30 °C (200 kPa absolute pressure of hydrogen on the anode side, and 100 kPa absolute pressure of nitrogen on the cathode side). The voltage range was between 0.05 and 1.0 V, at a scan rate of 50 mV s^{-1}. The voltage was scanned over 5 cycles, and the average spectra were obtained from the 2nd to 5th cycles. The electrochemical surface area (ECSA) was measured, and the mass activity (MA) was obtained by dividing current at 0.88 V by the mass of Pt. The specific activity (SA) was calculated by dividing the MA by the ECSA.

Results and Discussion

FCEV stack durability.—Figure 5 shows the results of the accelerated durability test at: (a) maximum power output (2.2 A cm^{-2}); and at (b) 12% power output (0.2 A cm^{-2}). The voltage drop relative to BOT was averaged from the voltage drops of all 13 cells in the stack. Initially, the fuel cell stack was subjected to start-stop cycling. After 30,000 start-stop cycles (EOT1), voltage drops of 1.4% (Fig. 5a) and 2.2% (Fig. 5b) were observed at 2.2 A cm^{-2} and 0.2 Acm^{-2}, respectively. The fuel cell stack was subsequently subjected to load cycling. After a further 73,000 load cycles (EOT2), total voltage drops of 5.3% (Fig. 5a) and 3.6% (Fig. 5b) were observed at 2.2 A cm^{-2} and 0.2 A cm^{-2}, respectively.

The voltage drop at 2.2 A cm^{-2} increases continuously and approximately linearly throughout the test. In contrast, at low current density (0.2 A cm^{-2}), the performance degradation slows down throughout the test, and appears to be plateauing by the end of the test. It is considered that not only deactivation of catalysts, but also deterioration of the catalyst layer by processes such as oxidation of the carbon support are expected to occur at higher current density. More detailed mechanisms of accelerated degradation at a high current density will be the subject of future studies. These results indicate that, in accelerated durability tests corresponding to a 15-year lifetime, the total voltage drop of the FCEV-ready stack is less than 6%. This already meets our tentative in-house goals set by the FCEV development program at Toyota, namely achieving a voltage drop below 8.8% at 2.2 A cm^{-2}, and below 7.7% at 0.2 A cm^{-2}.

Figure 6 shows the polarization curves at BOT (Fig. 6a), EOT1 (Figs. 6a and 6b), and EOT2 (Fig. 6b). From these results, it is evident that there is a greater voltage drop during the load cycle durability test (corresponding to greater deterioration) compared to during the start-stop cycle test, especially at a high current density. The degradation rate during the start-stop durability test at 2.2 A cm^{-2} was 3.3 $\times$ 10^{-4} mV per cycle (Fig. 6a) and the corresponding degradation rate during the load cycle durability test was 4.1 $\times$ 10^{-4} mV per cycle (Fig. 6b). These degradation rates are comparable, resulting in slightly larger voltage loss during the load cycling test compared to the start-stop test. This may be due to the greater number of total cycles and/or the higher cell temperature during the load cycle durability tests (Tables I and II).

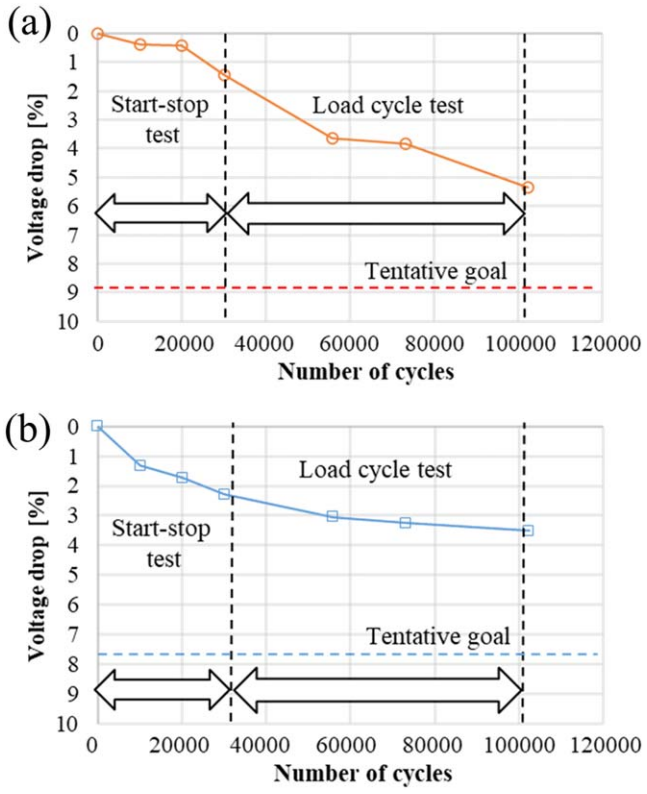

Figure 5. Magnitude of the voltage drop during the durability tests, measured at (a) 2.2 A cm^{-2} and (b) 0.2 A cm^{-2}.

Overall, these results confirm that prototype fuel cell stacks for mid-sized FCEVs already have sufficient durability in both start-stop and load cycle modes for practical applications.

Voltage at different cell positions.—It has been reported that different cell voltages can occur at different positions within fuel cell stacks, depending on the stack setup and operating conditions.[28] As such, we evaluated the voltage of each cell in the stack at BOT and EOT2, at 2.2 and 0.2 A cm^{-2}. The results for each of the 13 cells are shown in Fig. 7.

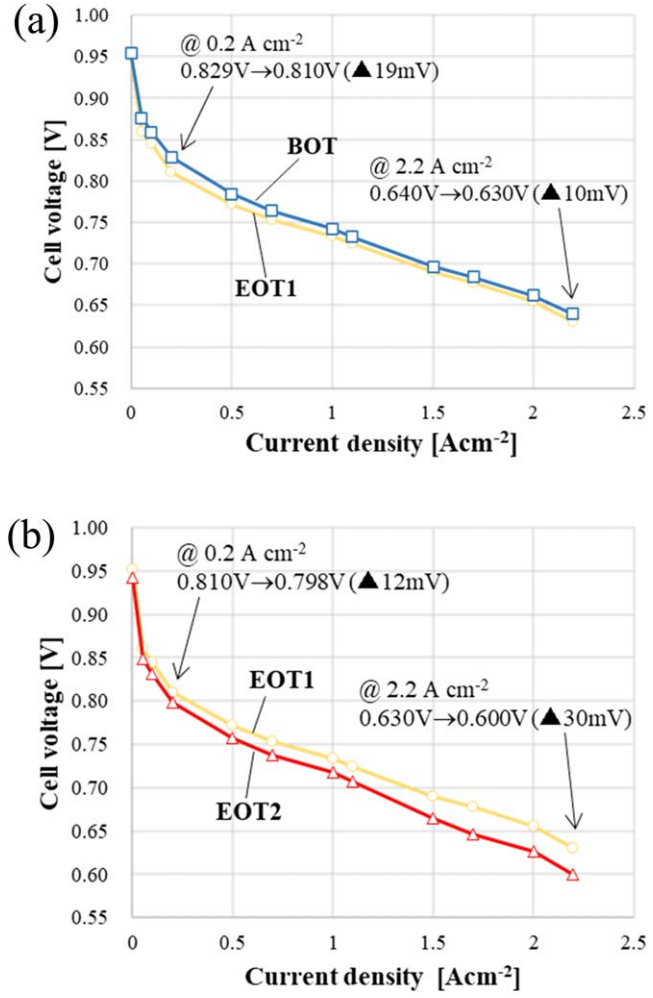

Figure 6. Current-voltage characteristics (a) at BOT (blue) and EOT1 (yellow); and (b) at EOT1 (yellow) and EOT2 (red). Immediately after the start-stop cycle durability test (EOT1), cell voltage drops of 19 mV at 0.2 A cm^{-2} and 10 mV at 2.2 A cm^{-2} were observed. After the subsequent load cycle durability test (EOT2), additional cell voltage drops of 12 mV at 0.2 A cm^{-2} and 30 mV at 2.2 A cm^{-2} were recorded.

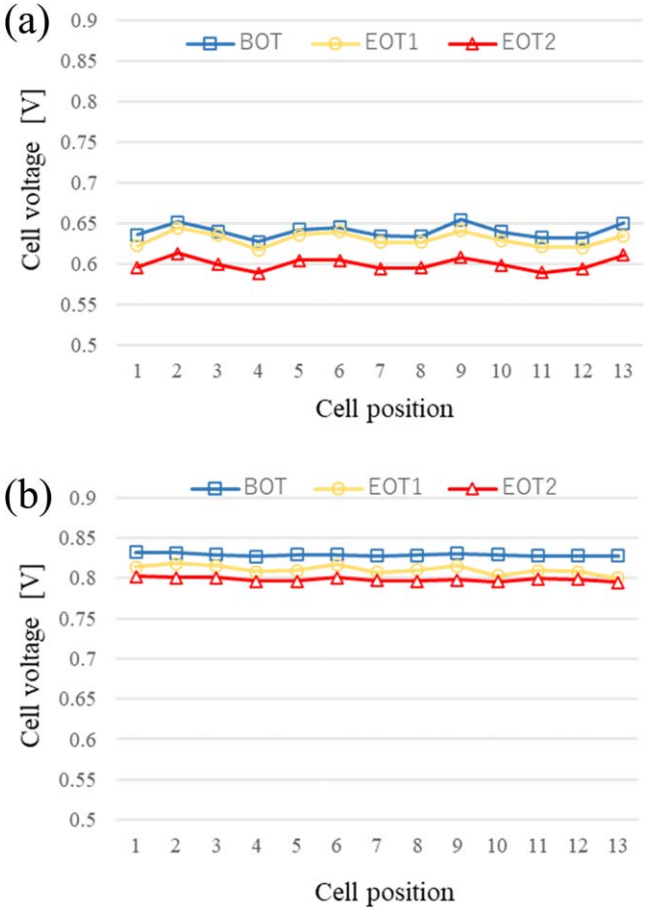

Figure 7. Position-dependent cell voltage at BOT (blue), after the start-stop durability test (EOT1, yellow), and after the subsequent load cycle durability test (EOT2, red), measured at either (a) 2.2 or (b) 0.2 A cm^{-2}.

At BOT, there is no remarkable difference in the cell voltage at different positions in the stack, and the standard deviation was just 8.2 mV, even at 2.2 A cm^{-2}. This indicates that a 13-cell stack for FCEVs exhibits negligible position-dependent voltage deviation. At EOT1, similar standard deviations of 8.5 mV at 2.2 A cm^{-2} were observed. Correspondingly, at EOT2, the standard deviations were 7.5 mV at 2.2 A cm^{-2}. Crucially, the standard deviation does not increase over the lifetime of the stack and is well within acceptable levels of variation. This means that degradation of prototype fuel cell stacks for FCEVs occurs uniformly across all the cells in the stack during the durability tests, confirming that the voltage drop does not depend on the cell position within the stack, in this case.

Overvoltage separation.—Separation of the different overvoltages in the stack can reveal valuable information about the degradation mechanisms and provide clues to improving FCEV performance. Here, the different overvoltages were separated from the polarization curves at BOT and EOT2, as shown in Fig. 8. The ohmic (IR) overvoltage was derived from the impedance data, and the IR-free cell voltage was derived from the polarization curves and the IR overvoltages. The IR overvoltages before ($V_{(IR)BOT}$) and after ($V_{(IR)EOT}$) durability tests, and the change in IR overvoltage between BOT and EOT ($\Delta V_{(IR)}$) were related via the following equations:

$$V_{(IR)BOT} = V_{(IR-free)BOT} - V_{(cell)BOT} \quad [1]$$

$$V_{(IR)EOT} = V_{(IR-free)EOT} - V_{(cell)EOT} \quad [2]$$

$$\Delta V_{(IR)} = V_{(IR)BOT} - V_{(IR)EOT} \quad [3]$$

Activation overvoltages were derived from the linear low current density region of the Tafel plots of IR-free voltages, as shown in Fig. 8b. The concentration overvoltage was inferred from the IR-free voltage and the activation overvoltage (Fig. 8b). Figure 9 shows the total increase in overvoltage (i.e., the voltage drop measured in the durability test) and the increase in each individual overvoltage at EOT2, relative to BOT, at 0.2 and 2.2 A cm^{-2}. It should be noted for clarity that these values represent the increases in overvoltages from BOT to EOT, rather than their absolute values. At BOT, the absolute IR overvoltages for the two different current densities were 9.2 mV at 0.2 A cm^{-2} and 93.6 mV at 2.2 A cm^{-2}, showing an approximately linear ohmic dependence. At EOT, the linear ohmic dependence was preserved, with absolute IR overvoltages of 10 mV at 0.2 A cm^{-2}, and 99.0 mV at 2.2 A cm^{-2}. From these values, the change in IR overvoltage from BOT to EOT is calculated to be 0.8 mV at 0.2 A cm^{-2}, and 5.4 mV at 2.2 A cm^{-2}, as shown in Fig. 9. In this case, the change in IR overvoltage does not follow a linear relationship, which could be caused by differences in the ohmic resistance of the ionomer depending on e.g. the current density or relative humidity,[41] or simply large experimental error due to the small numbers involved.

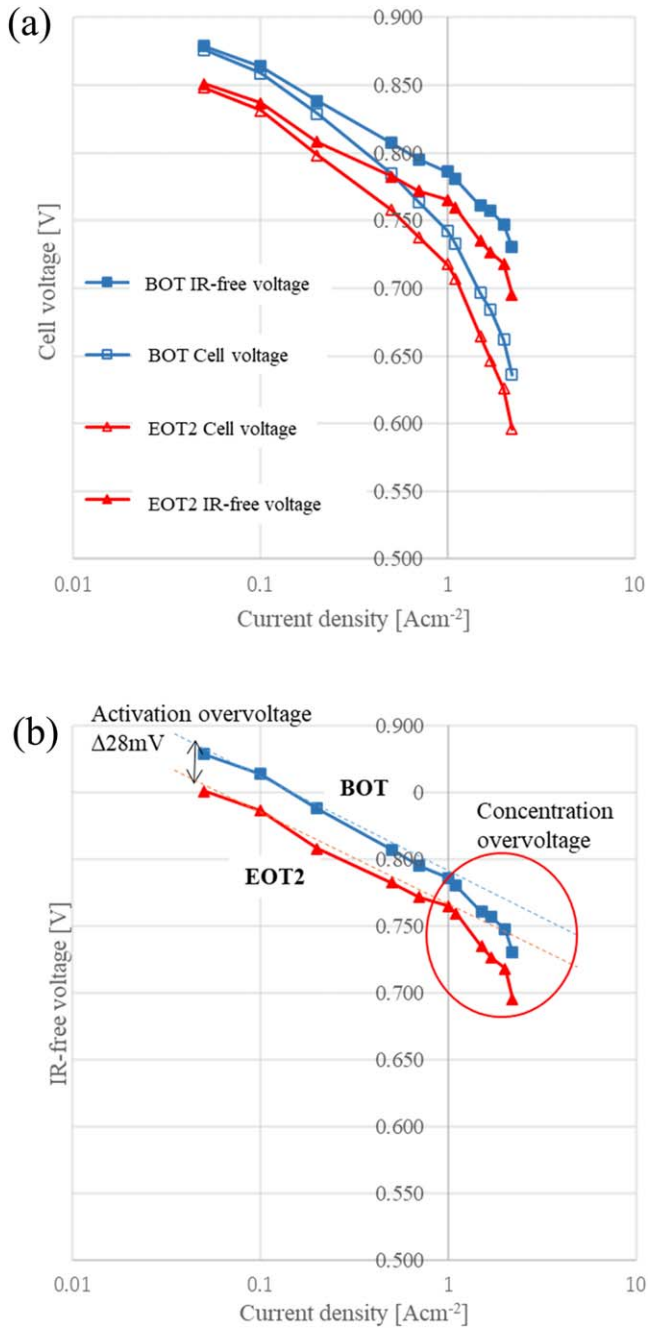

Figure 8. (a) Cell voltage and IR-free voltage at BOT and EOT2. (b) Comparison of the activation and concentration overvoltages obtained from the IR-free polarization curves at BOT and EOT2.

This figure shows that, at low current density (0.2 A cm^{-2}), the total increase in overvoltage from BOT to EOT2 was 31.0 mV, and the largest contribution to this by far was the increase in activation overvoltage (28.3 mV). Meanwhile, the increases in ohmic and concentration overvoltage were 0.8 mV and 1.7 mV, respectively, i.e., negligibly small. At high current density (2.2 A cm^{-2}), the total increase in overvoltage was slightly higher at just over 40 mV. Again, the largest contribution to this was the increase in activation overvoltage (28.3 mV). In this case, the contribution from both the ohmic and concentration overvoltages are larger than at low current density, at 5.4 and 6.5 mV, respectively. The reasons for these increases in overvoltages are explored in the following sections. However, according to the results, these overvoltage values are low enough to ensure sufficient stack performance for an FCEV, even after the severe durability test corresponding to normal operation over 15 years. It is concluded that negligible fuel cell degradation occurs during the accelerated stack durability tests.

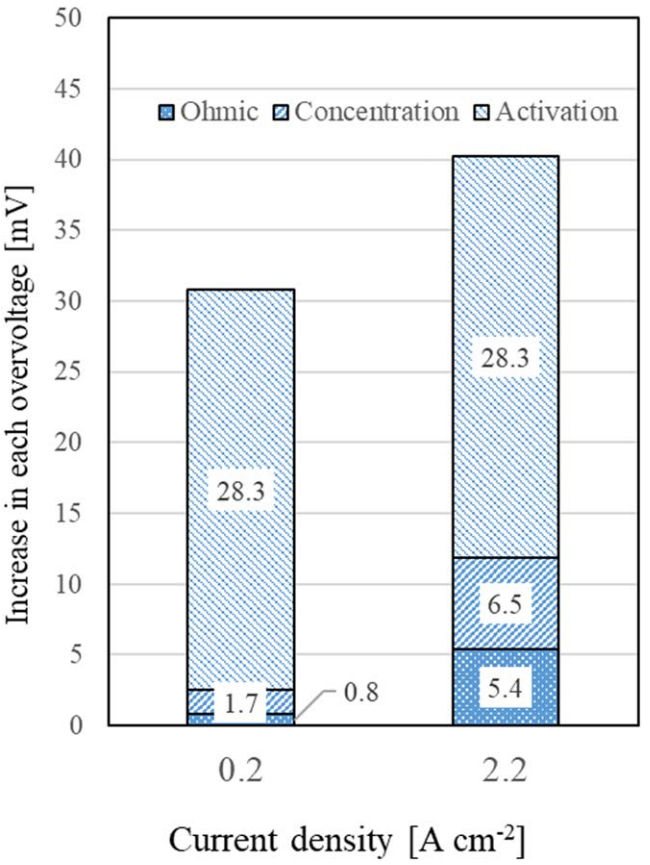

Figure 9. Total increase in overvoltage (voltage drop), and the increase in each overvoltage from BOT to EOT2, characterized at 0.2 and 2.2 A cm^{-2}.

Electrochemical Surface Area and Specific Activity.—To evaluate the catalytic activity before and after accelerated durability tests, cyclic voltammograms were recorded at BOT and EOT2, as shown in Fig. 10. The ECSA as determined from the hydrogen adsorption peak area in the cyclic voltammograms was 55.0 m^2 g^{-1} Pt at BOT, and this decreased to 37.4 m^2 g^{-1} Pt at EOT2, corresponding to 68% ECSA retention, as shown in Table IV. Meanwhile, the SA similarly decreased from 19.2 A m^{-2} Pt at BOT to 12.6 A m^{-2} Pt at EOT2, corresponding to 66% retention of activity, also shown in Table III. These decreases in ECSA and SA may be associated with e.g. platinum and cobalt dissolution, nanoparticle aggregation, and Ostwald ripening, causing an increase in activation overvoltage, as mentioned in the introduction.

According to our previous in-house experience, we have observed that there is an approximately linear correlation between the ECSA retention and the cell voltage retention after durability tests, as shown in Fig. 11.[5–13,35] According to this linear empirical relationship, an ECSA retention of 68% corresponds to a cell voltage retention of 96.46% at 0.2 A cm^{-2} (Fig. 11), and thus a voltage drop of 29 mV (3.54% decrease of 0.829 V at 0.2 A cm^{-2} in Fig. 6a). This empirical prediction is actually very close to the experimentally determined total overvoltage increase of 31 mV at 0.2 A cm^{-2} (Fig. 9). As such, this study provides verification for this empirical correlation, whilst more detailed analysis should be made to scientifically verify this relationship.

Meanwhile, cobalt ions from Pt-Co nanoparticles are known to leach into the ionomer layer during fuel cell operation, interfering with the proton conduction mechanisms via ion exchange and resulting in increased electrocatalyst layer resistance.[42,43] This is

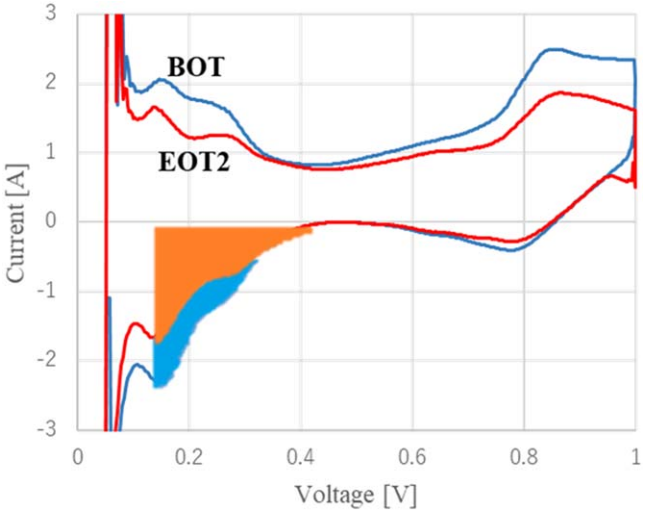

Figure 10. Cyclic voltammograms of a single full-size cell at BOT (blue) and EOT2 (orange). ECSA was derived from the hydrogen adsorption peak area specified in the figure.

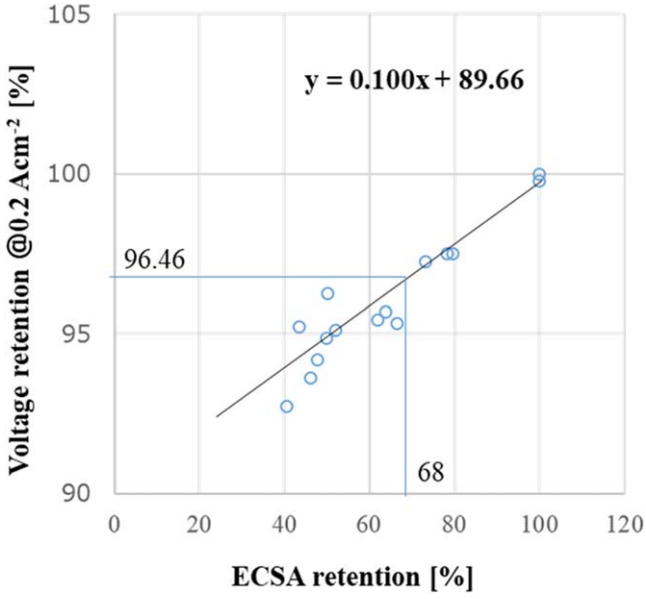

Figure 11. Relationship between the retention of ECSA (x in %) and retention of cell voltage at 0.2 A cm^{-2} (y in %).[35]

Table IV. Electrochemical surface area (ECSA) and specific activity (SA) at beginning of test (BOT) and end of test (EOT2), and the % retention of these parameters at EOT2. The SA is obtained by dividing mass activity (MA) by the ECSA. The MA (A g^{-1}) is obtained by dividing current at 0.88 V by the mass of Pt.

	ECSA [m^2 g^{-1} Pt]	SA [A m^{-2} Pt]
BOT	55.0	19.2
EOT2	37.4	12.6
Retention [%]	68	66

another potential contribution to the increase in ohmic overvoltage at EOT2. In addition, if cobalt contamination decreases the oxygen permeability of the ionomer, the concentration overvoltage may also be increased according to this phenomenon.

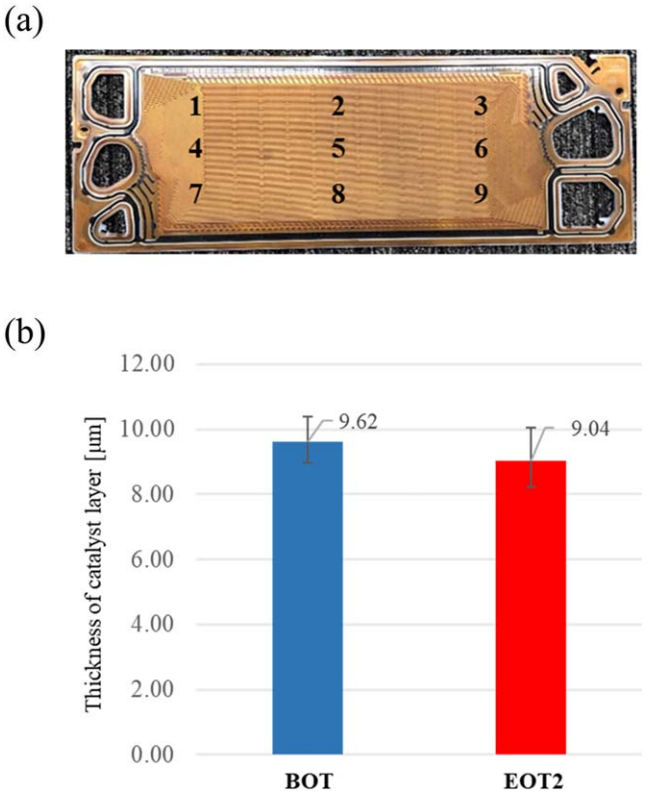

Figure 12. (a) Positions used for cathode electrocatalyst layer thickness measurements. (b) Average electrocatalyst layer thickness at BOT and EOT2.

Microstructural changes in the electrodes.—The thickness of the cathode electrocatalyst layer was determined by averaging measurements at 9 different locations on the electrode, as shown in Fig. 12a, at BOT and EOT2. The average thicknesses with their standard deviations are summarized in Fig. 12b. The results confirm that the thickness is slightly decreased at EOT2, by just 0.58 μm (i.e. 6%). This electrocatalyst layer thinning is generally attributed to oxidation and gasification of the carbon catalyst support. The thinning of the electrocatalyst layer is expected to interfere with the electron-conducting pathways. This agrees with the observed increase in ohmic overvoltage at EOT2. Indeed, the degree of electrocatalyst layer thinning is rather small, and this is also in agreement with the relatively small increase in ohmic overvoltage. In addition, electrode thinning could affect the tortuosity for gas transport, affecting the concentration overvoltage. Such thinning could also be caused by stack compression.

The microstructure of the electrocatalyst layers was also investigated. Figure 13 shows SEM micrographs of the Pt-Co alloy cathode catalysts decorated on the MCND carbon support at (a) BOT and (b) EOT2. Pt-alloy catalyst nanoparticles on the MCND support are seen in bright contrast. The average diameter of Pt-Co alloy particles clearly increased from 3.40 nm at BOT to 4.75 nm at EOT2, as shown in Table V. This 40% increase indicates aggregation and/or Ostwald ripening of the catalyst particles, providing an explanation for the observed increase in activation overvoltage at EOT2 as shown in Figs. 8 and 9. The average particle diameter at each of 5 different locations on the electrode were very similar, indicating that the highly uniform particle size distribution was maintained even throughout accelerated durability tests, without any dependence on the position in the stack.

The use of Pt-Co alloy cathode catalysts improves the catalytic activity compared to pure platinum, and dealloying of Co during the durability tests is a possible explanation for the observed drop in specific activity.[44] Detailed analysis of the Co content and the lattice

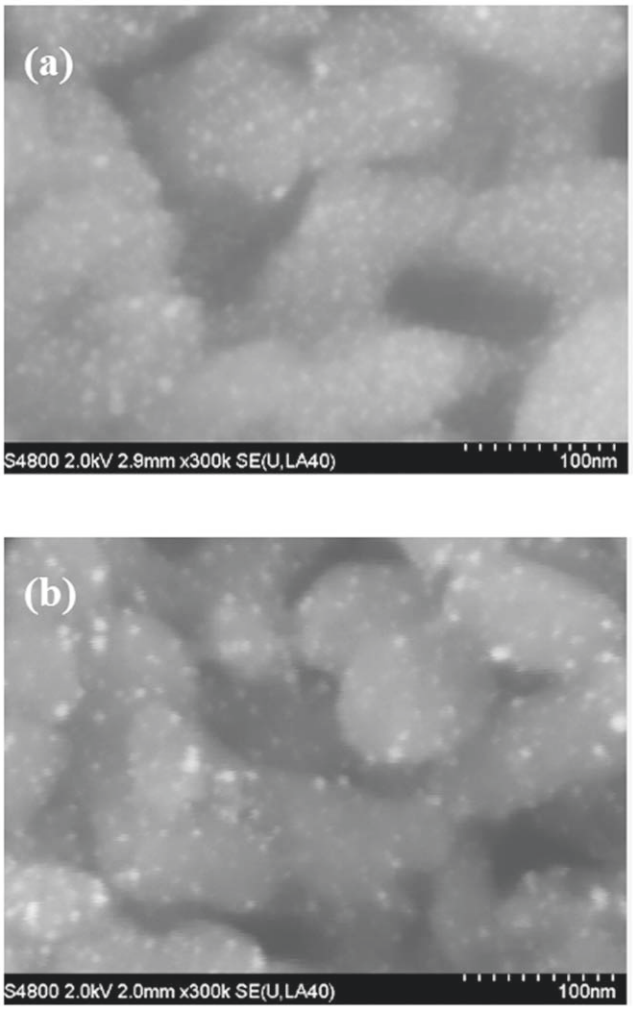

Figure 13. SEM micrographs of Pt-Co alloy catalysts decorated on the MCND carbon support at (a) BOT, and (b) EOT2.

Table V. Crystallite size of Pt-Co catalyst particles at EOT2, as determined by XRD analysis. Positions are specified in Fig. 12a.

Positions	Diameter [nm]
1	4.60
3	4.74
5	4.82
7	4.87
9	4.70
Average at EOT2	4.75
Average at BOT	3.40

parameters of the catalyst nanoparticles could lend insight into this issue, but are beyond the scope of this system-level study.

Conclusions

Modified accelerated durability tests with 30,000 start-stop cycles followed by 73,000 load cycles simulating realistic driving conditions were carried out on 13-cell prototype fuel cell stacks designed for commercial FCEVs. The 30,000 start-stop cycles correspond to switching the fuel cell system on and off on average 5 times a day over a period of 15 years. The 73,000 load cycles correspond to an acceleration event once every 2 to 3 km of driving, over a total driving range of 200,000 km. Even at maximum power density (2.2 A cm^{-2} in this study), the cell voltage dropped by less than 6%, successfully meeting durability targets for automotive applications, namely 15-year operation and 200,000 km driving range. In addition, the voltage drops occurred uniformly across all 13 cells. By separating the different contributions from the ohmic, activation, and concentration overvoltages, the degradation mechanisms were clarified. The largest contribution to stack degradation was from the activation overvoltage, which was attributed to Ostwald ripening and aggregation of platinum-based catalysts. The contribution from ohmic overvoltage was much smaller, and mainly attributed to electrocatalyst layer thinning, disrupting the electron conducing pathways, as well as Co ion dissolution reducing proton conductivity in the membranes and catalyst layers. A similarly small contribution to stack degradation was from the concentration overvoltage, attributed mainly to changes in tortuosity with electrode thinning. However, these degradation processes proceed well within tolerable limits for practical automotive fuel cell applications under normal operating conditions. Meanwhile, fuel cell system degradation under cold start and soak conditions is also of interest, and these will be investigated in a separate study. The above findings have been applied successfully in the development of new fuel cell systems for FCEVs, in particular the 2nd generation Toyota MIRAI.

ORCID

Yuya Tachikawa https://orcid.org/0000-0001-8003-0485
Akari Hayashi https://orcid.org/0000-0003-1753-2241
Kazunari Sasaki https://orcid.org/0000-0002-3174-9087

References

1. International Energy Agency, Energy Technology Perspectives 2017—Catalysing Energy Technology Transformations (2017), https://webstore.iea.org/energytechnology-perspectives-2017.
2. Hydrogen Council, Hydrogen, Scaling Up (2017), https://hydrogencouncil.com/wp-content/uploads/2017/11/Hydrogen-Scaling-up_Hydrogen-Council_2017.compressed.pdf.
3. K. Sasaki, H.-W. Li, A. Hayashi, J. Yamabe, T. Ogura, and S. M. Lyth, *Hydrogen Energy Engineering: A Japanese Perspective* (Springer, Japan) (2016).
4. International Energy Agency, The Future of Hydrogen - Seizing today's opportunities, Report prepared by the IEA for the G20, Japan (2019), https://iea.org/hydrogen2019/.
5. M. Kizaki, H. Asai, and H. Yumiya, *Toyota Technical Review*, **61**, 11 (2015).
6. T. Hasegawa, H. Imanishi, M. Nada, and Y. Ikogi, *SAE Technical paper*, **1**, 1185 (2016).
7. T. Maruo, M. Toida, T. Ogawa, Y. Ishikawa, H. Imanishi, M. Nada, and Y. Ikogi, *SAE Technical paper*, **1**, 1189 (2017).
8. N. Konno, S. Mizuno, H. Nakaji, and Y. Ishikawa, *SAE Int. J. Alt. Power*, **4**, 123 (2015).
9. A. Yamashita, M. Kondo, S. Goto, and N. Ogami, *SAE Technical paper*, **1**, 1169 (2015).
10. T. Takahashi, K. Kakeno, Y. Ikogi, and H. Imanishi, *Toyota Technical Review*, **66**, 12 (2021).
11. S. Mizuno, T. Hayashi, H. Kubo, M. Okumura, T. Kurihara, and K. Mori, *Toyota Technical Review*, **66**, 22 (2021).
12. T. Takahashi, *The Special Steel*, **70**, 11 (2021).
13. T. Takahashi, *J. Hydrogen Energy Systems Soc. Japan*, **46**, 135 (2021).
14. C. S. Gittleman, A. Kongkanand, D. Masten, and W. Gu, *Current Opinion Electrochem.*, **18**, 81 (2019).
15. R. L. Borup, A. Kusoglu, K. C. Neyerlin, R. Mukundan, R. K. Ahluwalia, D. A. Cullen, K. L. More, A. Z. Weber, and D. J. Myers, *Current Opinion Electrochem.*, **21**, 192 (2020).
16. H. A. Baroody and E. Kjeang, *J. Electrochem. Soc.*, **168**, 044524 (2021).
17. N. Ramaswamy, S. Kumaraguru, W. Gu, R. S. Kukreja, K. Yu, D. Groom, and P. Ferreira, *J. Electrochem. Soc.*, **168**, 024519 (2021).
18. R. K. Ahluwalia, X. Wang, J-K. Peng, V. Konduru, S. Arisetty, N. Ramaswamy, and S. Kumaraguru, *J. Electrochem. Soc.*, **168**, 044518 (2021).
19. EERE, Appendix D of DOE Solicitation DE-PS36-06GO96017 (2007), https://www1.eere.energy.gov/hydrogenandfuelcells/fuelcells/pdfs/component_durability_profile.pdf.
20. FCCJ, The membrane electrode assembly (MEA) durability test protocols, *Fuel Cell Commercialization Conference of Japan (FCCJ)* (2011), https://fccj.jp/pdf/23_01_kt.pdf.
21. A. Ohma, K. Shinohara, A. Iiyama, T. Yoshida, and A. Daimaru, *ECS Trans.*, **41**, 775 (2011).
22. Y. Hashimasa, Y. Matsuda, D. Imamura, M. Akai, and M. Sasaki, *Trans. JSME*, **77**, 147 (2011).
23. Y. Nakazato, D. Kawachino, Z. Noda, J. Matsuda, S. M. Lyth, A. Hayashi, and K. Sasaki, *J. Electrochem. Soc.*, **165**, F1154 (2018).

24. S. Matsumoto, M. Nagamine, Z. Noda, J. Matsuda, S. M. Lyth, A. Hayashi, and K. Sasaki, *J. Electrochem. Soc.*, **165**, F1164 (2018).
25. T. Tamaki, A. Koshiishi, Y. Sugawara, H. Kuroki, Y. Oshiba, and T. Yamaguchi, *J. Appl. Electrochem.*, **48**, 773 (2018).
26. J. Miyake, R. Taki, T. Mochizuki, R. Shimizu, R. Akiyama, M. Uchida, and K. Miyatake, *Sci. Adv.*, **3**, eaao0476 (2017).
27. C. Klose, M. Breitwieser, S. Vierrath, M. Klingele, H. Cho, A. Büchler, J. Kerres, and S. Thiele, *J. Power Sources*, **361**, 237 (2017).
28. M. Miller and A. Bazylak, *J. Power Sources*, **196**, 601 (2011).
29. S. Yamamoto, S. Sugawara, and K. Shinohara, 467 *Polymer Electrolyte Fuel Cell Durability* (Springer, New York, NY) (2009).
30. D. Batet, F. T. Zohra, S. B. Kristensen, S. J. Andreasen, and L. Diekhöner, *Appl. Energy*, **277**, 115588 (2020).
31. Y. Hashimasa and T. Numata, *Int. J. Hydrogen Energy*, **40**, 11543 (2015).
32. R. M. Darling and J. P. Meyers, *J. Electrochem. Soc.*, **150**, A1523 (2003).
33. R. M. Darling and J. P. Meyers, *J. Electrochem. Soc.*, **152**, A242 (2005).
34. P. J. Ferreira et al., *J. Electrochem. Soc.*, **152**, A2256 (2005).
35. T. Takahashi, Unpublished results.
36. T. Nagasawa, A. Nogi, T. Ikeda, S. Ikeda, S. Yano, S. Takeshita, and T. Itakura, *Toyota Technical Review*, **66**, 34 (2021).
37. S. Numao, K. Judai, J. Nishijo, K. Mizuuchi, and N. Nishi, *Carbon*, **47**, 306 (2009).
38. R. Jinnouchi, K. Kudo, K. Kodama, N. Kitano, T. Suzuki, S. Minami, K. Shinozaki, N. Hasegawa, and A. Shinohara, *Nature Comm.*, **12**, 4956 (2021).
39. Bts.gov, Vehicle miles traveled and vehicle trips by State, US Bureau of Transportation Studies (2017), https://bts.gov/statistical-products/surveys/vehicle-miles-traveled-and-vehicle-trips-state.
40. M. Tada, T. Uruga, and Y. Iwasawa, *Catalysis Lett.*, **145**, 58 (2015).
41. H. Nguyen, F. Lombeck, C. Schwarz, P. A. Heizmann, M. Adamski, H.-F. Lee, B. Britton, S. Holdcroft, S. Vierrath, and M. Breitwieser, *Sustainable Energy Fuels*, **5**, 3687 (2021).
42. R. K. Ahluwalia, D. D. Papadias, N. N. Kariuki, J.-K. Peng, X. Wang, Y. Tsai, D. G. Graczyk, and D. J. Myers, *J. Electrochem. Soc.*, **165**, F3024 (2018).
43. Y. Cui, Y. Wu, Z. Wang, X. Yao, Y. Wei, Y. Kang, H. Du, J. Li, and L. Gan, *J. Electrochem. Soc.*, **167**, 064520 (2020).
44. R. L. Borop, K. L More, and D. J. Myers, *FC-PAD: Fuel Cell Performance and Durability Consortium Update to USCAR Analysis of Toyota Mirai Components Provided by USCAR*, LA-UR-24454, Department of Energy (2018), https://www.osti.gov/biblio/1440417-fc-pad-fuel-cell-performance-durability-consortium-update-uscar-analysis-toyota-mirai-components-provided-uscar.